

# Initial Experimental Results of Three-Dimensional Plasma Structure Reconstructed from Seven Independent X-Ray Images on RELAX

Shinichiro INAGAKI, Akio SANPEI, Takeru INOUE and Haruhiko HIMURA

*Department of Electronics, Kyoto Institute of Technology, Matsugasaki, Sakyo Ward, Kyoto 606-8585, Japan*

(Received 25 November 2022 / Accepted 19 January 2023)

In this study, we demonstrated the principle underlying the three-dimensional (3D) reconstruction of plasma structure by using a soft X-ray camera with multiple pinholes. Time evolutions of seven independent soft X-ray images were captured by the camera. The obtained data were used to reconstruct a 3D soft X-ray emission profile in the reversed-field pinch produced in the RELAX machine, which appeared to be consistent with the forecast in our feasibility study.

© 2023 The Japan Society of Plasma Science and Nuclear Fusion Research

Keywords: imaging measurement, reversed-field pinch, soft X-ray, three-dimensional diagnostics

DOI: 10.1585/pfr.18.1202010

Spontaneous nonaxisymmetric deformations of plasma have been observed not only in stellarators but also in tokamaks and reversed-field pinches (RFPs) [1]. Therefore, a method to monitor the plasma in three dimensions (3D) is required to investigate the transitions leading to deformations. The feasibility of monitoring the plasma structure by using a “multiple-pinhole camera” was examined in a previous study [2], which entailed numerical tests on the reconstruction of emission profiles. In this paper, we present the preliminary results of our experimental investigation into the 3D profile of soft X-ray (SXR) emissivity by using the multiple-pinhole camera attached to the RELAX machine [3].

RELAX has a torus vacuum chamber with major  $R$  and minor  $a$  radii that are 508 and 250 mm, respectively. The cross-section of the chamber is circular. The multiple-pinhole camera used to view toroidal plasmas in RELAX from the equatorial plane of the chamber, through one of four ICF152 viewing ports located radially around the chamber. Figure 1 shows the experimental setup of the measurement system along with a cross-sectional view of the multiple-pinhole camera. The multiple-pinhole camera consists of seven pinholes, an aperture, and a microchannel plate (MCP) containing a phosphor plate. Seven pinholes were drilled into a disk located at  $y = 945$  mm, with the origin of the coordinate system being the center of the torus. The  $y$ -axis lies along the optical axis of the camera. One of the pinholes was drilled at the center of the disk, while the others were uniformly distributed on the circumference of a circle centered on the disk and having a radius of 5.3 mm.

Each pinhole has a diameter of 0.5 mm and were covered by a  $1\ \mu\text{m}$  thin film made of aluminum. The aper-

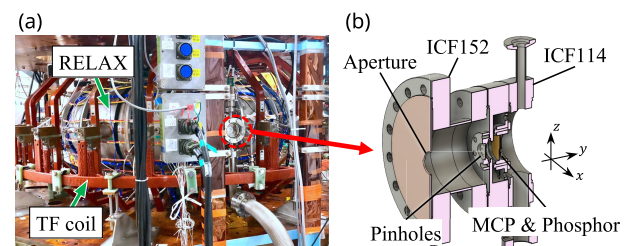


Fig. 1 (a) A photograph of the area near the ICF152 viewing port, where the multiple-pinhole camera is attached, and (b) a cross-sectional view of the multiple-pinhole camera.

ture has a diameter of 20 mm, and was placed at a distance of 57.4 mm from the disk with pinholes. The MCP and the phosphor plate attached to it have diameters of 20 and 17 mm, respectively. The distance between the MCP and the disk with pinholes is 14.7 mm. As a result, each angle of view of the pinholes and the entire angle of view of the camera are approximated to be  $20^\circ$  and  $30^\circ$ , respectively. The boundary of the field of view are illustrated by a dashed black lines in Fig. 2.

The time evolution of SXR images was obtained by converting SXRs into visible light using the phosphor plate attached to the MCP. Images that appeared on the phosphor plate were captured by a high-speed camera (Photron FASTCAM SA-4). The camera had a shutter speed of 100 kfps, and the images were recorded on a  $192 \times 128$  pixel array with a dynamic range of 12 bits. Before image processing, the obtained images were cropped and resized to a  $32 \times 32$  pixel to effectively magnify the original image. Each pixel is approximated to be a square with dimensions of 0.52 mm. As a result, the spatial resolution on the mid-plane is approximated to be 16.5 mm per pixel at  $y = 508$  mm (which is the same as  $R$ ).

author's e-mail: m1621009@edu.kit.ac.jp

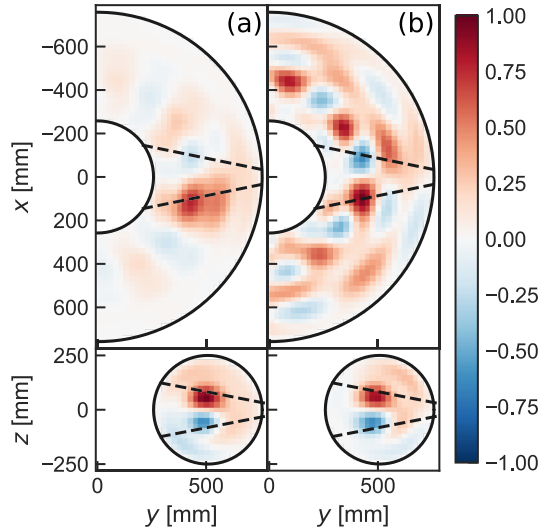


Fig. 2 Cross-sectional views of the 3D emission profile of SXR calculated by using (a) Ridge and (b) Lasso regressions. Black dashed lines indicate the boundary of the field of view from the camera.

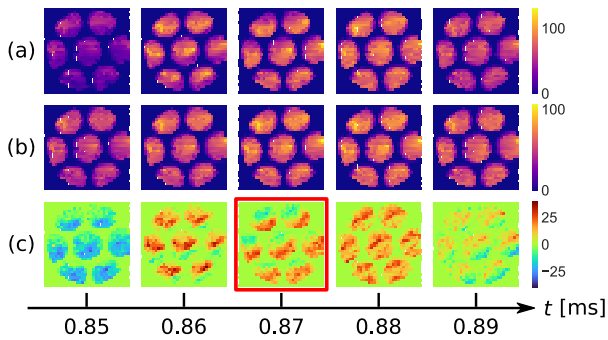


Fig. 3 (a) Time evolution of the images captured by the multiple-pin-hole camera, (b) moving average obtained from the filmed images, and (c) the resultant image calculated by subtracting (b) from (a). A clear asymmetric structure is observed.

In the experiments, consecutive images were captured during the quasi-steady state of RFPs with a plasma current of approximately 65 kA. Figure 3 (a) shows a typical set of time evolution images. To clearly extract luminous intensity corresponding to the asymmetry shape of the plasma core, we create artificial images using a moving average method over five images before and after each measured image, as shown in Fig. 3 (b). These images reflect the axisymmetric component of SXR, as plasmas are believed to rotate in the toroidal direction [4]. The resultant image obtained by subtracting (b) from (a) at each time is shown in Fig. 3 (c). A helical shape is clearly visible in the image at  $t = 0.87$  ms in Fig. 3 (c), which is highlighted by a red square.

The image corresponding to  $t = 0.87$  ms in Fig. 3 (c) may be compared with the forecast from Ref. [2]. We follow the strategy used in Ref. [2], and employ the Fourier–

Bessel series expressed as:

$$f_{m,k,n}^{(c/s)}(r, \theta, \phi) = \begin{cases} J_m(\lambda_k^m r) \cos(m\theta + n\phi) \\ J_m(\lambda_k^m r) \sin(m\theta + n\phi) \end{cases}, \quad (1)$$

$$\begin{aligned} f(r, \theta, \phi) &= \sum_{m,k,n} \left\{ s_{m,k,n}^{(c)} f_{m,k,n}^{(c)} + s_{m,k,n}^{(s)} f_{m,k,n}^{(s)} \right\} \\ &= \sum_i s_i f_i(r, \theta, \phi), \end{aligned} \quad (2)$$

where all the parameters in Eqs. (1) and (2) are defined in the Ref. [2], except for the range of  $m$  and  $n$ . For the image at  $t = 0.87$  ms in Fig. 3 (c), the values of  $m$  fall in the range  $0 \leq m \leq 2$ , and the values of  $n$  fall in the range  $-8 \leq n \leq 8$ . Prior studies have shown that the dominant mode numbers of the observed magnetic perturbations are  $m = 1$  and  $n = -4$  or  $-5$  [4]. Amplitude of modes with  $|n| > 8$  were negligible. Moreover,  $k$  is limited to the range of  $1 \leq k \leq 3$  to avoid alias in images outside the field of view. Furthermore, the  $K$ -fold cross-validation method [2] with  $K = 8$  was used to determine a suitable regularization parameter  $\alpha$ , as explained in the Ref. [2].

Resultant cross-sectional profiles obtained by using Ridge and Lasso regressions [2] are shown in Figs. 2 (a) and (b), respectively. The color bar represents the normalized emissivity of SXR. While a unique periodicity of the normalized intensity appears outside the field of view in the  $xy$  plane of Fig. 2 (a), a clear periodicity in the normalized intensity can be recognized in Fig. 2 (b). Such a non-uniformity appears in the  $yz$  plane for both cases, which strongly suggests the presence of the helical core in the plasma. Since the camera captures inverted images of the plasma, higher emission of SXR occurs at the lower right corner of the obtained image in the case. Figure 3 (c) also suggests that the helical core appears to rotate over time, indicating plasma rotation. While further analyses are required to establish these findings, the 3D reconstruction of plasma core using the SXR camera with multiple pinholes apparently works well in actual experiments.

The authors would like to thank Ms. N. Kojima, Mr. R. Takaoka, and Mr. T. Sasaki for their help in running the RELAX machine. We also acknowledge Mr. E. Kai for his first sketch of the multiple-pin-hole. We would like to thank Editage ([www.editage.com](http://www.editage.com)) for editing the manuscript. This work was supported by JSPS KAKENHI No. 20KK0063 and No. 21H01056 and by the National Institute for Fusion Science No. NIFS22KIPP016 and No. NIFS20KOAP035, and, in part, by the Joint Usage/Research Program on Zero-Emission Energy Research, Institute of Advanced Energy, Kyoto University ZE2022A-24.

- [1] L. Marrelli *et al.*, Nucl. Fusion **61**, 023001 (2021).
- [2] S. Inagaki, A. Sanpei and H. Himura, Nucl. Instrum. Methods Phys. Res. A **1036**, 166857 (2022).
- [3] S. Masamune *et al.*, J. Phys. Soc. Jpn. **76**, 123501 (2007).
- [4] K. Oki *et al.*, Plasma Fusion Res. **7**, 1402028 (2012).